Improving the Flux Pinning With Artificial BCO Nanodots and Correlated Dislocations in YBCO Films Grown on IBAD-MgO Based Template

Mukarram Z. Khan, Yue Zhao, X. Wu, Rajveer Jha, Veer P. S. Awana, Hannu Huhtinen, and Petriina Paturi

***Abstract*—To improve the performance of high-temperature superconductors in electrical power systems, a modified IBAD-MgO based template is used as a substrate for the growth of $YBa_2Cu_3O_{6+x}$(YBCO) doped with various concentrations of $BaCeO_3$ (BCO). The highest critical current density (J_c) in a wide applied field and angular range is realized in the films doped with 2% and 4% BCO content. This is explained to arise from the optimized BCO dopant concentration, which helps to immobilize more vortices both in low and high field ranges. Besides the vortex pinning by randomly distributed BCO nanoparticles, the edge-type dislocations, mainly occurring due to the underlying IBAD-MgO based template, are also a main source of pinning the vortices as seen by the appearance of *c*-axis peak of $J_c(\theta)$ in undoped and 2% doped films. The disappearance of c-peak in films doped with higher concentration can be qualitatively explained by the vortex path model, where the paths of the vortices arising because of high density of BCO particles disguise the columnar type pinning effect coming from the threading dislocations within the films. Therefore, the BCO nanodots can be used for improving the flux pinning besides the threading dislocations in YBCO films on metal substrates.**

***Index Terms*—HTS, YBCO, BCO, flux pinning, angular dependent properties.**

I. Introduction

THE high temperature superconductor $YBa_2Cu_3O_{6+x}$ (YBCO) has already shown its potential in electrical power systems when deposited on flexible buffered metallic substrates [1]. Thinner metallic templates are of immense importance as they reduce the production cost but, on the other hand, a better understanding about YBCO growth on such types of templates is also necessary. As the vortex motion causes dissipation in high temperature superconductors, the pinning of vortices is always desired, especially at high fields where vortex density is quite high [2]. For J_c enhancement in YBCO films grown by pulsed laser deposition (PLD), several non-superconducting phases such as $BaCeO_3$ [3], $BaZrO_3$ [4] or $BaSnO_3$ [5] have been successfully doped as they create pinning sites for the mobile vortices. Based on the lattice mismatch calculations between YBCO matrix and dopant species as well as the elastic constants of the pinning centers, as presented in detail in [6], it is expected that BCO forms non-columnar and spherical particles when grown by PLD. This is also confirmed by TEM analysis, where the point-like BCO particles with a mean diameter of 2.5 nm are observed in 4% BCO doped YBCO films [3].

In this manuscript, our objective is to enhance the J_c in YBCO films when grown on an advanced IBAD-MgO based template by PLD via doping $BaCeO_3$ (BCO). By PLD method, the BCO dopant grows within the YBCO matrix in the form of isotropic and randomly distributed nano-sized particles [3]. For this purpose, the dopant content is optimized within YBCO films deposited on our IBAD-MgO based template. We discuss the structural, magnetic and transport properties of small-scale YBCO films grown at a specific temperature. The main objective is to study the vortex pinning behavior in undoped and BCO doped YBCO films and then to optimize the dopant content for J_c enhancement, when grown on our IBAD-MgO based template.

II. Experimental Details

The YBCO thin films doped with the varying content of non-superconducting phase BCO were prepared by PLD on 5×5 mm^2 IBAD-MgO based templates where the dopant concentration was varied from 0 vol% to 10 vol% with 2 vol% steps. The schematic of IBAD-MgO based template is shown in Fig. 1 and its manufacturing details are explained in [7]. The IBAD-MgO layer not only forms the in-plane grain alignment but is also biaxially textured. Furthermore, the low lattice mismatch, good chemical compatibilty and similar thermal expansion coefficient values between the CeO_2 cap layer and YBCO are important for the optimal growth of YBCO [7]. All the films were deposited at growth temperature $T_g = 750$ °C by using excimer XeCl laser (wavelength = 308 nm, pulse duration = 25 ns and pulse repetition rate = 5 Hz with 1.3 Jcm^{-2} laser fluence). The number of 1500 laser pulses with the growth rate

Manuscript received October 23, 2018; accepted January 31, 2019. Date of publication February 4, 2019; date of current version March 4, 2019. This work was supported in part by the Jenny and Antti Wihuri Foundation and in part by the Finnish Cultural Foundation. *(Corresponding author: Mukarram Z. Khan.)*

M. Z. Khan is with the Wihuri Physical Laboratory, Department of Physics and Astronomy, University of Turku, Turku FI-20014, Finland, and also with the University of Turku Graduate School, University of Turku , Turku FI-20014, Finland (e-mail: mukarram.z.khan@utu.fi).

Y. Zhao is with the Department of Electrical Engineering, Shanghai Jiao Tong University, Shanghai 200240, China.

X. Wu is with the Shanghai Superconductor Technology Company Ltd., Shanghai 200240, China.

R. Jha and V. P. S. Awana are with the Superconductivity Division, National Physical Laboratory (CSIR), New Delhi 110012, India.

H. Huhtinen and P. Paturi are with the Wihuri Physical Laboratory, Department of Physics and Astronomy, University of Turku, Turku FI-20014, Finland.

Color versions of one or more of the figures in this paper are available online at http://ieeexplore.ieee.org.

Digital Object Identifier 10.1109/TASC.2019.2897433

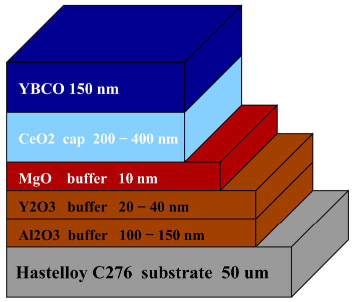

Fig. 1. The schematic structure of IBAD-MgO based polycrystalline metallic substrate, different buffer layers and their thicknesses. The 150 nm thick layer of undoped or BCO doped YBCO was deposited on top of it.

of 0.1 nm/pulse gave us 150 nm film thickness. The detailed PLD deposition conditions are explained elsewhere [8].

The crystallographic properties of films were determined by Philips X'Pert Pro MPD based X-ray diffraction (XRD). The phase purity of films was confirmed by (00l) directional θ-2θ scans whereas the calculations of in-plane and out-of-plane crystallographic textures were made by YBCO (102) (ϕ scans) and (005) (ω scans) peaks, respectively. The Quantum Design physical property measurement system (PPMS) was used for magnetic measurements where critical temperatures T_c of the films were determined by ac magnetization measurements between 10 K−100 K in 0.1 mT ac field. The critical current densities (J_c) were calculated by applying Bean model for films onto the respective hysteresis loops [9]. The accommodation field B*, which is defined as an upper limit of the low-field plateau of J_c(B), is determined by the criterion $J_c(B)/J_c(0) = 0.9$ [10]. On the other hand, the angular dependent transport properties were also done by the use of the horizontal rotator in PPMS. Firstly, all the films were patterned by wet chemical etching to produce 200 μm wide current stripes on each film. Then TPT HBO5 Wire Bonder was used to make electrical contacts on films by aluminium wire. The measurements were made at 40 K and magnetic fields of 0.5 T, 1 T, 2 T, 4 T, 6 T and 8 T with 0° to 360° angular range using 3° of steps.

III. Results and Discussion

A. Structural Properties

All the films are phase pure as shown in Fig. 2 by the relative (00l) peaks of YBCO and other peaks coming from buffer layers of our IBAD-MgO based template. The calculated structural parameters of undoped and BCO doped YBCO are presented in Table I. The c-axis length is nearly the same for all the films and is also very close to the nominal value of YBCO c-parameter i.e. 11.68 Å [11]. However, we observed the increase in $\Delta 2\theta$ values with increasing BCO concentration, which could be linked not only to the strain related variation in c-parameter but also to the out-of-plane lattice coherence length [12].

On the other hand, the in-plane variation of all the films, as depicted by $\Delta\phi$ data, stays approximately the same regardless of the dopant content. The $\Delta\phi$ values are quite large as compared with the STO case which suggests the formation of low-angle grain boundaries along c-direction [13]. Moreover, the intensity ratio of the (005) and (004) peaks $I(005)/I(004) < 20$ in all the films indicates that the oxygen deficiency is in the range of standard $\delta < 0.1$ [14].

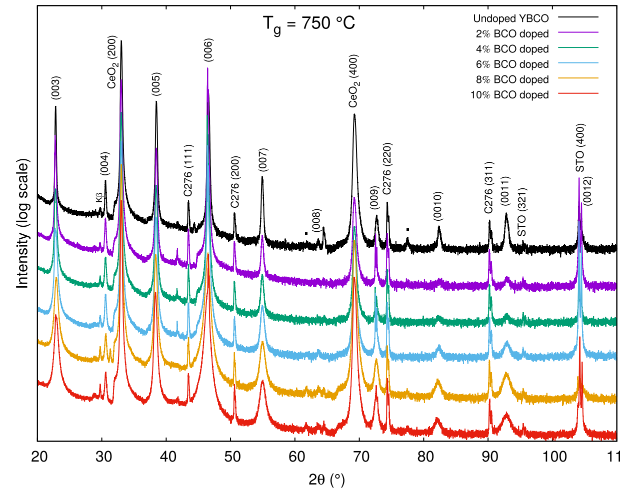

Fig. 2. X-ray diffractograms of undoped and 0% to 10% BCO doped YBCO films grown on a modified IBAD-MgO based template. Labelled peaks, CeO_2 are from cap layer, '·' peaks arose from the buffer layers and C276 peaks reflected from the metal itself. STO peak is also seen due to hastelloy tape glued on it.

TABLE I
Structural Parameters Determined From XRD Measurements of Undoped and Several Concentrations of BCO Doped YBCO Films Grown on IBAD-MgO Based Template

Sample	YBCO lattice c (Å)	$\Delta 2\theta$ (005) (°)	$\Delta\phi$ (102) (°)	I(005)/ I(004)
Undoped	11.69	0.21	4.12	13.12
2% BCO	11.68	0.25	4.16	10.87
4% BCO	11.70	0.30	4.09	11.77
6% BCO	11.69	0.32	4.09	12.86
8% BCO	11.69	0.39	4.09	15.46
10% BCO	11.69	0.39	3.97	15.41

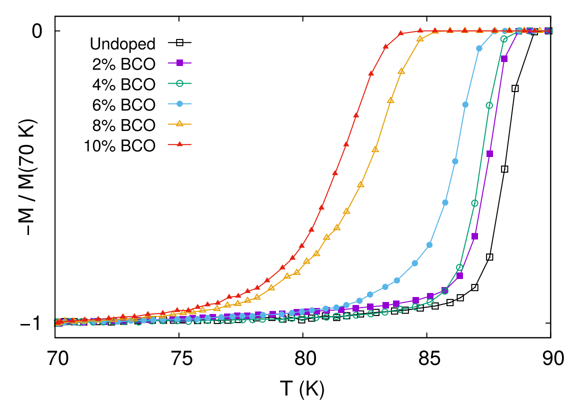

Fig. 3. AC magnetization curves as a function of T for undoped and BCO doped YBCO films grown on an IBAD-MgO based template.

B. Magnetic Analysis

Temperature dependent ac-magnetization curves in Fig. 3 show that the T_c decreases as the BCO dopant concentration increases. It can be observed that the undoped film has the

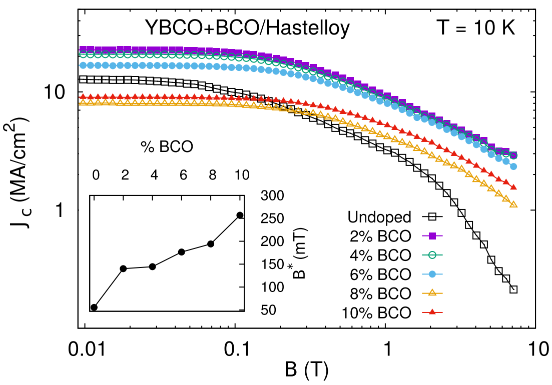

Fig. 4. J_c curves as a function of zero and applied magnetic fields measured at 10 K for undoped and BCO doped YBCO films deposited on an IBAD-MgO based template at $T_g = 750$ °C. The inset shows the accommodation field (B^*) dependence on BCO dopant concentration.

highest T_c and with increasing dopant concentration it starts to decrease which is a typical behavior observed in BCO doped YBCO films [15]. In addition, above 4% dopant content, the width of the transition increases as well as the T_c drops dramatically above 6% dopant concentration. The decrease in T_c with increasing BCO doping can be explained by the formation of non-uniform strain which is directly proportional to the structural deformation of YBCO [3], [16].

J_c s in all the films, depicted in Fig. 4, were calculated using the Bean model [9], [17], [18]. The 2% BCO doped film has the highest J_c whereas the 4% BCO doped has slightly lower J_c in self-field. In high field or above accommodation field B^*, both 2% and 4% doped films have approximately the same J_c s. Above 4% dopant concentration i.e. with 6% BCO doped film, the decrease of self-field J_c is notable while the high field J_c decreases more slowly. This result can be explained by the high density of strong pinning sites due to 6% BCO concentration which pin more number of vortices. Above 6% dopant content the decrease of J_c, both in low and high fields, is remarkable as the film structure gets deteriorated with such a high dopant concentration which affects negatively the superconducting properties. On the other hand, the undoped YBCO has higher self-field J_c than 8% and 10% BCO doped films but lower in high fields. The lower self-field J_c in highly BCO doped YBCO films can be linked to the increased volume of BCO particles and distorted YBCO surroundings with lower T_c, which together decrease the amount of superconducting material [16]. In addition, the inset of Fig. 4 revealing the dependence of B^* on BCO dopant concentration shows that the undoped YBCO film has the lowest B^* and then it jumps three times higher when doped with 2% and 4% BCO. Above 4% dopant content B* increases almost linearly and this behavior is similar as observed in our works [3], [15].

C. Angular Dependent Flux Pinning

Figure 5 shows the angular dependent J_c properties for all the films with respect to different fields. When comparing absolute $J_c(\theta)$ values, we observed that $J_c(\theta)$ increases from undoped to 2% BCO doped film in entire angular range and up to the higher field too. This means that the isotropic BCO nanoparticles pin the vortices effectively especially in high fields with high vortex density. At 4% dopant content, the absolute value of low field $J_c(\theta)$ stays approximately the same as of 2% dopant concentration but high field $J_c(\theta)$ is slightly decreased. Moreover, the c-peak in fields above 2 T decreases slightly, thus showing that the pinning force lacks the local maximum in the c-direction [19] but there is still c-axis oriented pinning. With 6% BCO concentration, the highest $J_c(\theta)$ is observed in low fields among all of our samples, but at the high fields, the $J_c(\theta)$ is even smaller than in the undoped one. Above 6% BCO doped films, the properties start to worsen in the whole field and angular ranges as 10% BCO doped film has even smaller absolute $J_c(\theta)$ than the 8% doped one. The decline of superconducting properties with high dopant concentration is due to excess structural disorder in the film. This matches our structural and magnetic analysis described in previous sections. The c-axis peak arising in undoped or BCO doped films and the slight off position of c-peak from 0° is a typical behavior when YBCO is grown on IBAD-MgO based template [20]–[22]. As YBCO grows c-oriented, the appearance of c-peak in this case is due to threading dislocations which occur because of growth mechanism of underlying IBAD-MgO based template [22]. These dislocations also act as pinning sites and increase $J_c(\theta)$ [13].

The anisotropy in all of our data is related to the density of pinning paths along in-plane and out-of-plane directions. A strong anisotropy is seen when the pinning paths are more populated in one direction than in the other i.e. usually the undoped films have more pinning paths along the ab-plane than the c-direction [23], [24]. Moreover, the effects of the matching field are also responsible for the anisotropic shapes of the curves [25].

The proposed model about the interaction of vortices with threading dislocations and isotropic and randomly distributed BCO particles is presented in Fig. 6. The pronounced appearance of c-peak in undoped and 2% BCO doped films could be due to the trapping of the entire length of vortices by edge-type dislocations, which are formed in the low-angle grain boundaries, caused by the underlying IBAD-MgO based template [13]. When the dopant concentration is 2%, only a few BCO particles in the vicinity of threading dislocations will pin the vortices. However, the isotropic BCO particles are not very effective to pin the vortices in all the angular directions and therefore only the threading dislocations can accomodate the vortices for longer length. Thus, the pinning by BCO nanoparticles together with threading disloacations increases $J_c(\theta)$ as shown by Fig. 5 (b). When the concentration is increased up to 4%, the extra BCO particles will start attracting the vortices, not allowing them to be directly pinned in the threading dislocations. This phenomenon already reduces the c-peak in 4% BCO doped film. In addition, the curves of 4% BCO doped film are the least anisotropic among all of our measured data. This behavior is more pronounced when the BCO concentration is increased to 6%, where the c-peak is already reduced. On the other hand, the 8% and 10% BCO doped films have quite many short vortex pinning paths in between the BCO nanoparticles which not only completely hide the c-peak but, due to the effect of the high

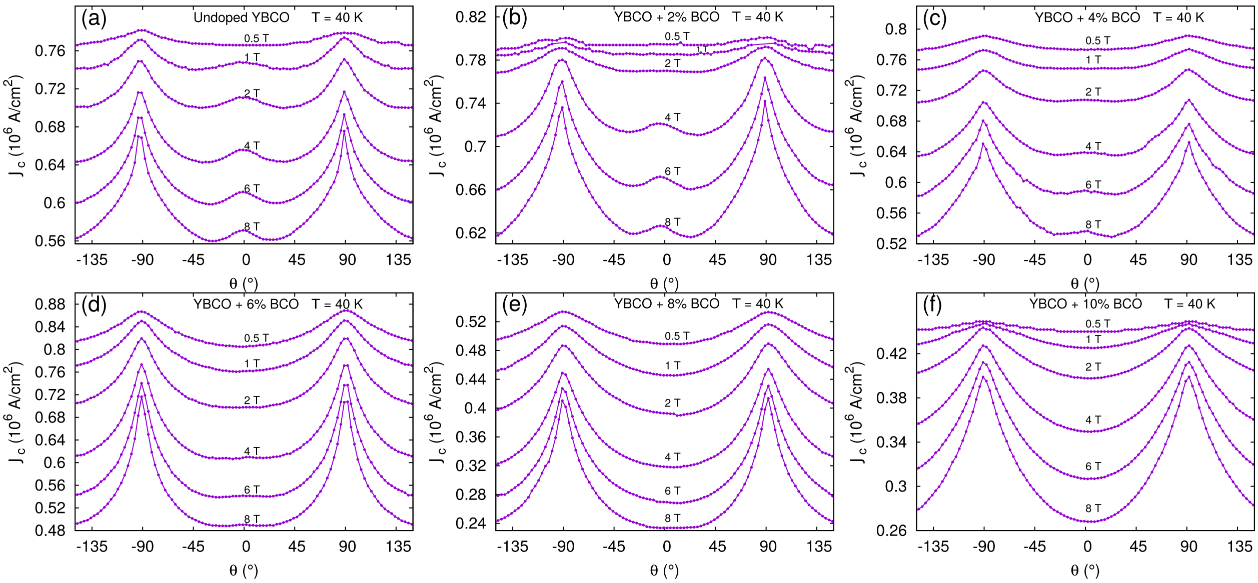

Fig. 5. (a)–(f) The angular dependent J_c plots for undoped and BCO doped YBCO films grown on IBAD-MgO based template measured at 40 K in field range of 0.5 T−8 T. All the graphs were shifted so that 0° always shows the direction of c-axis while −90° and 90° refer to ab-planes in the YBCO structure.

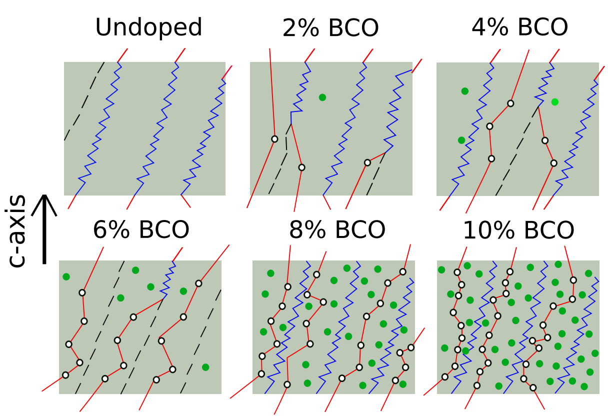

Fig. 6. The schematic of vortex pinning in undoped and 2% to 10% BCO doped YBCO films grown on an IBAD-MgO based template. Black dashed lines correspond to the threading dislocations where no vortex is pinned, whereas blue zig-zag color depicts the pinned vortices within threading dislocations. The green and open circles are BCO produced nanodots where the vortices (red lines) are unpinned and pinned, respectively. In the undoped case, vortices are mobile in between the threading dislocations unlike the BCO doped films where they are trapped by nanodots.

content of dopants, also reduce the absolute $J_c(\theta)$. As the vortices are lengthy, we conclude that the optimized low BCO dopant concentration is the best for making them immobile in between the threading dislocations. However, in the undoped case, not all of the vortices can be pinned by threading dislocations but only some of them, and thus especially at high fields, the great number of vortices move freely within the film which lowers the high field J_c.

IV. Conclusion

An advanced IBAD-MgO based template was used to grow undoped and 2% to 10% BCO doped YBCO films by PLD. The template consists of thinner and modified buffer layers reducing also its production cost. In this work, we optimized the BCO doping concentration in YBCO matrix in terms of vortex pinning. The low-angle grain boundaries, formed due to our IBAD-MgO based template, effectively pin the vortices and increase J_c. According to our results, the 2% and 4% doped films had the best $J_c(\theta)$ in all magnetic fields. These results are significant when optimizing the vortex pinning landscape in wide magnetic field and entire angular ranges and therefore, these structures can be used in future coated conductors for electrical power applications.

References

[1] V. Selvamanickam et al., "High-temperature superconductors for electric power and high-energy physics," *J. Minerals, Metals Mater. Soc.*, vol. 50, pp. 27–30, 1998.

[2] S. R. Foltyn et al., "Materials science challenges for high-temperature superconducting wire," *Nature Mater.*, vol. 6, pp. 631–642, 2007.

[3] M. Malmivirta et al., "The angular dependence of critical current of $BaCeO_3$ doped $YBa_2Cu_3O_{6+x}$ thin films," *IEEE Trans. Appl. Supercond.*, vol. 25, no. 3, Jun. 2015, Art. no. 6603305.

[4] J. L. MacManus-Driscoll et al., "Strongly enhanced current densities in superconducting coated conductors of $YBa_2Cu_3O_{7-x}$+$BaZrO_3$," *Nature Mater.*, vol. 3, pp. 439–443, 2004.

[5] P. Mele et al., "Systematic study of the $BaSnO_3$ insertion effect on the properties of $YBa_2Cu_3O_{7-x}$ films prepared by pulsed laser ablation," *Supercond. Sci. Technol.*, vol. 21, 2008, Art. no. 125017.

[6] J. Wu and J. Shi, "Inetractive modeling-synthesis-characterization approach towards controllable *in situ* self-assembly of artificial pinning centers in re-123 films," *Supercond. Sci. Technol.*, vol. 30, 2017, Art. no. 103002.

[7] Q.-Q. Mu, L.-F. Liu, and Y.-J. Li, "Fabrication of IBAD-MgO and PLD CeO_2 layers for YBCO coated conductors," *Chin. Phys. Lett.*, vol. 32, 2015, Art. no. 078102.

[8] H. Palonen, H. Huhtinen, M. A. Shakhov, and P. Paturi, "Electron mass anisotropy of $BaZrO_3$ doped YBCO thin films in pulsed magnetic fields up to 30 T," *Supercond. Sci. Technol.*, vol. 26, 2013, Art. no. 045003.

[9] H. P. Wiesinger, F. M. Sauerzopf, and H. W. Weber, "On the calculation of J_c from magnetization measurements on superconductors," *Physica C*, vol. 203, pp. 121–128, 1992.

[10] C. Cai, B. Holzapfel, J. Hänisch, L. Fernandez, and L. Schultz, "Magnetotransport and flux pinning characterictics in RBaCuO (R = Gd, Eu, Nd)

and ($Gd_{1/3}$ $Eu_{1/3}$ $Nd_{1/3}$)BaCuO high-T_c superconducting thin films on $SrTiO_3$," *Phys. Rev. B*, vol. 69, 2004, Art. no. 104531.

[11] P. Schweiss *et al.*, "Static and dynamic displacements in $RBa_2Cu_3O_{7-\delta}$ (R = Y, Ho; $\delta = 0.05, 0.5$): A neutron-diffraction study on single crystals," *Phys. Rev. B*, vol. 49, pp. 1387–1396, 1994.

[12] A. Gauzzi and D. Pavuna, "Quantitative analysis of growth-induced reduction of long range lattice order in ion-beam sputtered $YBa_2Cu_3O_{6.9}$ films," *Appl. Phys. Lett.*, vol. 66, pp. 1836–1838, 1995.

[13] M. Z. Khan, Y. Zhao, X. Wu, M. Malmivirta, H. Huhtinen, and P. Paturi, "Improved interface growth and enhanced flux pinning in YBCO films deposited on an advanced IBAD-MgO based template," *Physica C*, vol. 545, pp. 50–57, 2018.

[14] J. Ye and K. Nakamura, "Quantitative structure analyses of YBCO thin films: Determination of oxygen content from x-ray-diffraction patterns," *Phys. Rev. B*, vol. 48, pp. 7554–7564, 1993.

[15] M. Irjala, H. Huhtinen, R. Jha, V. P. S. Awana, and P. Paturi, "Optimization of the $BaCeO_3$ concentration in YBCO films prepared by pulsed laser deposition," *IEEE Trans. Appl. Supercond.*, vol. 21, no. 3, pp. 2762–2766, Jun. 2011.

[16] M. Peurla *et al.*, "Optimization of the $BaZrO_3$ concentration in YBCO films prepared by pulsed laser deposition," *Supercond. Sci. Technol.*, vol. 19, pp. 767–771, 2006.

[17] C. P. Bean, "Magnetization of high-field superconductors," *Rev. Modern Phys.*, vol. 36, pp. 31–39, 1964.

[18] C. P. Bean and J. D. Livingston, "Surface barrier in type-II superconductors," *Phys. Rev. Lett.*, vol. 12, pp. 14–16, 1964.

[19] L. Civale *et al.*, "Angular-dependent vortex pinning mechanisms in $YBa_2Cu_3O_7$ coated conductors and thin films," *Appl. Phys. Lett.*, vol. 84, pp. 2121–2123, 2004.

[20] B. Maiorov *et al.*, "Influence of tilted geometries on critical current in superconducting thin films," *IEEE Trans. Appl. Supercond.*, vol. 15, no. 2, pp. 2582–2585, Jun. 2005.

[21] B. Maiorov, B. Gibbons, S. Kreiskott, V. Matias, T. Holesinger, and L. Civale, "Effect of the misalignment between the applied and internal magnetic fields on the critical currents of tilted coated conductors," *Appl. Phys. Lett.*, vol. 86, 2005, Art. no. 132504.

[22] S. H. Wee, Y. L. Zuev, C. Cantoni, and A. Goyal, "Engineering nanocolumnar defect configurations for optimized vortex pinning in high temperature superconducting nanocomposite wires," *Sci. Rep.*, vol. 3, pp. 23101–23109, 2013.

[23] N. J. Long, N. M. Strickland, and E. F. Talantsev, "Modeling of vortex paths in HTS," *IEEE Trans. Appl. Supercond.*, vol. 17, no. 2, pp. 3684–3687, Jun. 2007.

[24] N. J. Long, "Model for the angular dependence of critical currents in technical superconductors," *Supercond. Sci. Technol.*, vol. 21, 2008, Art. no. 025007.

[25] S. Wimbush and N. Long, "The interpretation of the field angle dependence of the critical current in defect-engineered superconductors," *New J. Phys.*, vol. 14, 2012, Art. no. 083017.